Am J Otolaryngol 40 (2019) 197–204

Contents lists available at ScienceDirect

Am J Otolaryngol

journal homepage: www.elsevier.com/locate/amjoto

Computational fluid dynamics analysis of H-uvulopalatopharyngoplasty in obstructive sleep apnea syndrome☆

Lei Zhu[a,1], Haibo Liu[a,1], Zhongying Fu[b], Jianmei Yin[b,*]

[a] The Emergency Department, the first hospital of Jilin university, Changchun, 130000, Jilin Province, China
[b] The Department of Otolaryngology-Head and Neck Surgery, The First Hospital of Jilin University, Changchun, 130000, Jilin Province, China

ARTICLE INFO

Keywords:
Uvulopalatopharyngoplasty
Obstructive sleep apnea syndrome
Computer simulation
Airway resistance
Pressure drop

ABSTRACT

Purpose: To explore the impact of H-uvulopalatopharyngoplasty (H-UPPP) in obstructive sleep apnea syndrome (OSAS) and gain insights into the potential mechanism underlying improvement by H-UPPP.

Methods: In a cohort of 11 OSAS patients, computational fluid dynamics (CFD) models of the upper airway were obtained using commercial software from computed tomography (CT) datasets before and after H-UPPP. Morphological and numerical parameters were respectively computed and compared during the peak tidal inspiratory flow. The correlations among polysomnography endpoints, airway dimensions, and pre- and post-operative airflow properties were analyzed with Spearman's rank correlation.

Results: The preoperative minimum cross-sectional area was significantly increased by 89.56% ($p < .05$), with a positive correlation to the apnea hypoapnea index (AHI) ($r = 0.974$). However, the capacity of all pharyngeal regions was not significantly altered ($p > .05$). Following H-UPPP, we observed a significant increase in pressure and reduction of velocity ($p < .05$) in the previously constricted areas. The change in pressure and velocity were significantly correlated with AHI ($r = 0.922$ and $r = 0.946$, respectively). In addition, the pressure drop in the constricted area, oropharynx, and hypopharynx were also significantly decreased ($p < .05$).

Conclusions: H-UPPP is capable of expanding the constricted region of the velopharynx and can decrease the airway resistance which will in turn decrease the workload necessary for breathing and facilitate inspiration.

1. Introduction

Obstructive sleep apnea syndrome (OSAS) is a common chronic condition characterized by repetitive episodes of apnea and hypopnea during sleep resulting from partial or complete collapse of the upper airway which is induced by negative pressure inspiration [1]. Nocturnal polysomnography (PSG) is the standard technique used for the diagnosis of OSAS [2]. PSG is based on the simultaneous monitoring of sleep parameters as well as the cardiac and respiratory events. In the United States, it was recently estimated that the prevalence of OSAS is 2–4% among the adult population [3], In China, the prevalence rates is 4.63% [4]. OSAS is associated with diminished quality of life, higher cardiovascular and cerebrovascular risks, excessive daytime somnolence, traffic accidents, and increased health care costs [5].

To date, several approaches have been proposed for the treatment of OSAS including continuous positive airway pressure (CPAP) therapy, risk factor modification strategies like weight loss, oral appliances that advance the mandible or tongue during sleep, and diverse surgical manipulations that expand the upper airway [6]. Uvulopalatopharyngoplasty (UPPP) is a frequently used surgical procedure for the treatment of OSAS [7]. UPPP involves the excision of excessive tissues in the throat that include the uvula, the soft palate, and the tonsils [3]. Over the years, the UPPP procedure has undergone several modifications to enhance its efficacy [8]. Owing to the collapsibility of the lateral pharyngeal walls, the modified UPPP (H-UPPP) procedure was developed. H-UPPP partially or totally retains the uvula to prevent globus pharyngeus; thus leading to higher success rates [8–10]. Previous studies investigating the mechanism of UPPP were mainly confined to morphological changes in 2D or 3D images without focusing on the potential functional variations [11,12]. Computational fluid

☆ Statement of grant or other support
There is no grant or other support.

* Corresponding author at: The Department of Otolaryngology-Head and Neck Surgery, The First Hospital of Jilin University, No. 3302, Jilin Road, Erdao District, Changchun City, Jilin Province 130000, China.
E-mail addresses: lifeislife2005@jlu.edu.cn (L. Zhu), yinjianmei1985@jlu.edu.cn (J. Yin).
[1] Lei Zhu and Haibo Liu contributed equally to this paper.

https://doi.org/10.1016/j.amjoto.2018.12.001
Received 14 October 2018

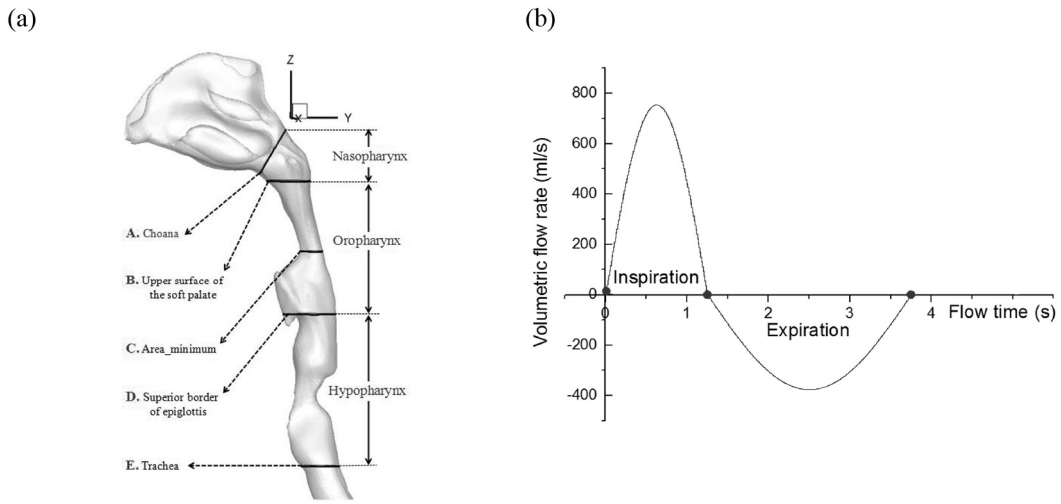

Fig. 1. (a) The upper airway was divided into five transverse planes resulting into the division of the upper airway into nasal cavity, nasopharynx, oropharynx, and hypopharynx. (b) A typical flow input waveform for transient flow in the respiratory cycle.

dynamics (CFD) has been extensively used in biomedical research to study fluid flow. Accumulating evidence confirmed that the CFD-derived endpoints based on the pressure drop (ΔP) of pharyngeal cavity were more closely associated with severity of OSAS than the corresponding anatomical endpoints [13–16]. Therefore, CFD can be a superior alternative technique to evaluate airway collapsibility. To this end, in the present study we aimed to investigate the impact of H-UPPP on OSAS outcome using CFD simulation and further examine the potential mechanisms underlying the observed improvement of OSAS following H-UPPP.

2. Methods

2.1. Subjects

A total of 11 patients (9 males, 2 females) presented with OSAS were recruited from the departments of Otolaryngology and Head and Neck Surgery, The First Hospital of Jilin University between April 2016 and December 2017. All experiments were in accordance with the ethical standards of the Institutional Review Board and Ethics Committee of the First Hospital of Jilin University and the 1964 Helsinki declaration and its later amendments or comparable ethical standards. An informed written consent was obtained from all participants included in the study.

Patients were diagnosed with either moderate ($n = 3$) or severe ($n = 8$) OSAS according to the data obtained from overnight polysomnography (PSG) as described previously [17]. Following diagnosis, all patients were required to perform a full upper respiratory airway computed tomography (CT) scan a month before H-UPPP. Next, they underwent an H-UPPP procedure by experienced surgeons [18]. Six months after the H-UPPP, patients were required to repeat the upper airway CT scan. Exclusion criteria included: (1) Severe craniofacial deformity, (2) Age under 18 years old, (3) History of cardiovascular events or acquiring serious medical illnesses during treatment like cardiovascular disorders or respiratory system diseases like chronic obstructive pulmonary disease or asthma or severe nasal conditions like nasal septum deviation, (4) Previous surgical treatments for OSAS.

2.2. Model construction and data transfer

Pre- and post-operative CT scans were obtained on a 64-row multidetector scanner (Brilliance CT, Philips Medical Systems, Cleveland, OH, USA). Patients were asked to keep their heads and necks in the Frankfort horizontal position parallel to the floor and close their mouths with the tongues touching their hard palates [19]. Subsequently, CT datasets were imported into a commercial software package (Mimics Medical 17.0, Materialise, Belgium), and the anatomical geometric models were reconstructed. Finally, the geometries were exported into a reverse engineering software package (Geomagic Studio 2014, 3D Systems Inc., USA) and the 3D models were converted into non-uniform rational B-splines surfaces. Then, those models were transferred to Hyperworks 13.0 (Altair Engineering, Inc., Auckland, New Zealand) to generate an unstructured tetrahedral volume mesh.

2.3. CFD analysis

The numerical simulation of flow field from pre- and post-operative CT scans of the upper respiratory airway were respectively analyzed utilizing a commercial CFD package (Fluent 17.0, ANSYS Inc.) as discussed previously [20]. A transient 3D incompressible laminar flow field was conducted to simulate the whole respiratory cycle. The respiratory tidal volume was set at 600 ml with a respiratory rate of 16 breaths per minute. Next, rhinomanometry was used to assess the patency of the nasal airway through measuring the air pressure and airflow rate during breathing [21]. The rhinomanometer test showed that the sinusoidal breathing pattern expressed by the airflow rate as a function of time and the ratio of inspiration as well as the expiration times was 1:2. The velocity boundary condition at the nostril of an inlet was set to piecewise sinusoidal function by compiling the user-defined functions (Fig. 1, b): 753 ml/s (peak of inspiration), and - 377 ml/s (peak of expiration). Meanwhile, pressure boundary condition is set as zero at the outlet. In terms of material properties, the density of air was 1.225 kg/m^3, and the viscosity was assumed to be 1.789×10^{-5} kg/m/s. A non-slip boundary condition at the airway wall was applied and the time step $\Delta t = 0.001$ s was adopted.

2.4. Analysis of the CFD post-processing variables

Data files generated by Fluent 17.0 software were transferred into the visual software package (Tecplot 360 EX 2015, Tecplot Inc.) for the CFD post-processing analysis [22]. Four transversal planes (A, B, D, and E) were identified according to the anatomical landmarks, which resulted in dividing the whole pharynx into three parts (nasopharynx, oropharynx, and hypopharynx) (Fig. 1a). The minimum cross-sectional area and its location (plane C) were defined by implementing an integral algorithm. Finally, a median sagittal plane was obtained in the longitudinal direction of the model. The three-dimensional coordinates of the above-mentioned six cross-sections were shared in the pre- and

postoperative models. Next, the upper airway morphology was inspected and the oropharynx was designated as the region of our interest. The variation of the oropharyngeal volume and the minimum cross-sectional area across the *Z*-axis were evaluated as described previously [14]. In addition, the degree of pharyngeal stenosis was determined as detailed previously [15]. Briefly, the percentage of the pharyngeal stenosis (PPS) was calculated from the following formula that compared the value of minimum cross-sectional area ($Area_C$) with the size at the upper surface of soft palate ($Area_B$).

$$Percentage\ of\ pharyngeal\ stenosis\,(PPS) = \left(1 - \frac{Area_C}{Area_B}\right) \times 100\% \quad (1)$$

Additionally, the amelioration of pharyngeal constriction after H-UPPP was estimated using the above-mentioned formula from the postoperative model.

During sleep, negative pressure leading to airway collapse is closely associated with inspiration [14]. Therefore, we analyzed the change of the flow field through extracting the model data and contour of above-mentioned planes at the peak of inspiration (inhalational velocity at the nostril was 753 ml/s) [23,24]. Specifically, this study focused on examining the pressure and velocity along the pharynx such as the area-weighted average pressure (AWAP) and velocity (AWAV). Then, the pressure drop (ΔP) from the choana to each plane and pressure difference of pharyngeal regions ($\Delta P_{(nasopharynx)}$, $\Delta P_{(oropharynx)}$, and $\Delta P_{(hypopharynx)}$) were calculated.

The pre- and post-operative curves using the mean difference in pressure (ΔP) from the pharyngeal regions and the change of volume flow rate (Q) during inspiration were constructed [25]. Next, the effective resistance of airway (R) was calculated from the mean slope of the fitted lines using the formula

$$R = \frac{\Delta P}{Q} \quad (2)$$

Next, we computed the wall shear stress to better understand the frictional resistance of airway as described previously [26]. Subsequently, we analyzed the rate of change to predict the extent of variation of all parameters. The rate of change was defined as the difference between pre- and post-operative variables ($Variable_{pre}$ & $Variable_{post}$) divided by the absolute value of the corresponding pre-operative parameters (3).

$$\text{Rate of change} = \frac{Variable_{post} - Variable_{pre}}{|Variable_{pre}|} \times 100\% \quad (3)$$

Finally, the correlations between changes of apnea-hypopnea index (AHI), variations of morphology, and alterations of airflow properties were analyzed with Spearman correlation coefficient. Paired *t*-tests were used to compare the flow profiles and the different anatomical parameters of the upper airway before and after H-UPPP. *A p* value < .05 was considered to be statistically significant.

3. Results

3.1. Clinical features and surgical outcome

A total of 11 patients (9 males and 2 females; age 35.27 ± 5.37 years and BMI 34.17 ± 1.39 kg/m^2) diagnosed with moderate to severe OSAS were enrolled in this study. All patients underwent a standard H-UPPP where the uvula was preserved and a larger portion of the soft palate and bilateral tonsils were removed, allowing maintenance of the normal anatomy of the soft palate [18]. Six months after the H-UPPP, all patients demonstrated significant improvement in the OSAS parameters including the AHI, apnea index, mean oxygen saturation, lowest oxygen saturation, and oxygen desaturation index ($p < .05$; Table 1).

Table 1
Clinical features before and after H-UPPP procedure (Mean ± SD, $n = 11$).

Parameter	Preoperative	Postoperative	P value*
Age(years)	35.27 ± 5.37	35.27 ± 5.37	n/a
Gender (M/F)	9(M), 2(F)	9(M), 2(F)	n/a
BMI (kg/m^2)	34.17 ± 1.39	33.78 ± 1.12	0.146
AHI	58.34 ± 6.24	11.49 ± 1.95	0.000†
AI	37.18 ± 5.06	2.30 ± 0.32	0.000†
Mean SaO_2 (%)	87.82 ± 0.70	92.09 ± 0.64	0.000†
Lowest SaO_2 (%)	49.73 ± 2.91	69.36 ± 1.91	0.000†
ODI	53.59 ± 1.96	7.27 ± 0.69	0.000†

BMI = body mass index; AHI = apnea-hypopnea index; AI = apnea index; SaO_2 = oxygen saturation; ODI = oxygen desaturation index; M = Male; F = Female.
*Based on Paired *t*-test.
† Statistically significant ($p < .05$).

3.2. Airway morphology

Following H-UPPP procedure, the cross sectional area of plane C increased significantly (12.15 ± 0.47 vs 6.46 ± 0.20, $p < .05$, Table 2). Additionally, we observed a significant positive correlation between the H-UPPP procedure and AHI ($r = 0.974$; Table 2). Moreover, compared to the pre-surgical conditions, PPS was significantly improved after H-UPPP procedure (52.06% vs 74.66%, *respectively* $p < .05$; Table 2). Similarly, a significant positive correlation with AHI was also observed ($r = 0.948$; Table 2). Meanwhile, the volumes of the nasopharynx and hypopharynx showed insignificant variations, the volumetric changing rate of each was 0.06% ($p = .805$) and 0.68% ($p = .101$), respectively. Additionally, the mean oropharyngeal volume was increased by 8.53% after H-UPPP ($p = .069$). The volumetric variables were weakly correlated to AHI.

3.3. CFD simulation and H-UPPP outcome

Following H-UPPP, the mean AWAP values were increased in each representative plane (Table 3). Compared to the pre-operative AWAP value, AWAP values showed the largest increase in plane C (−153.54 ± 6.18 vs −69.95 ± 2.50; % of change = 53.65%, $p < .05$; Table 3), with a significant correlation to AHI ($r = 0.922$). On the other hand, we did not observe a significant difference in the mean AWAP at the choana ($p = .130$) and the correlation to AHI was insignificant ($r = 0.101$). Those variations of pressure were further validated in the pre- and post-operative representative model contours (Fig. 2). Additionally, the difference in pressure (ΔP) from the choana to each plane was decreased (Table 3 and Fig. 3a). Interestingly, the largest decline in the post-operative ΔP were observed in planes C and D (66.81% and 71.79%, respectively; $p < .05$) with a positive correlation with AHI ($r = 0.928$ and $r = 0.874$, respectively). Similarly, the largest decline in the post-operative pressure drop was observed in the oropharynx (Fig. 3b).

Next, we investigated the change of the AWAV (Table 3 and Fig. 4). Except for the choana plane, the speed of inspiration was decreased across the transverse planes A, B, C, and D. The post-operative AWAV values were significantly decreased in planes C and D (42.07% and 9.59%, respectively; $p < .05$). In contrast, the change of AWAV in planes B and E was insignificant (0.92% and 0.27%, respectively; $p > .05$). In plane C, the change in velocity was significantly correlated with AHI ($r = 0.946$). Finally, differences of streamlines suggested that H-UPPP made possible variation of the airflow pattern (Fig. 4c + d). Following H-UPPP, the oropharyngeal unsteady airflow state was inhibited; instead, we observed a laminarized airflow due to the elimination of airway constriction.

For a deeper insight into the impact H-UPPP on upper airway resistance, the pre- and post-operative ΔP-Q curves were constructed (Fig. 5). The effective airway resistance, R, was detected from the slope

Table 2
Comparison of the morphological variables before and after H-UPPP, and their correlations to the change in AHI (Mean ± SD, n = 11).

Variables	Preoperative	Postoperative	%Change*	*P* value**	r value (vs. AHI)
A_{min}	6.46 ± 0.20	12.15 ± 0.47	89.56 ± 8.56	0.000†	0.974
PPS (%)	74.66 ± 1.60	52.06 ± 3.58	−30.84 ± 3.83	0.000†	0.948
$V_{nasopharynx}$	6.09 ± 0.20	6.07 ± 0.17	−0.06 ± 1.19	0.805	0.295
$V_{oropharynx}$	9.80 ± 0.39	10.67 ± 0.63	8.53 ± 4.14	0.069	0.251
$V_{hypopharynx}$	15.41 ± 1.30	15.31 ± 1.30	−0.68 ± 0.41	0.101	0.398

A_{min} = minimum cross-sectional area; AHI = apnea-hypopnea index; PPS = percentage of the pharyngeal stenosis; $V_{nasopharynx,\ oropharynx,\ hypopharynx}$ = volume of nasopharynx, oropharynx, hypopharynx.
*Postoperative rate of change relative to the preoperative variable.
**Based on paired *t*-test.
† Statistically significant ($p < .05$).

Table 3
Comparison of CFD variables between before and after H-UPPP procedure, and their correlations to AHI (Mean ± SD, n = 11).

Sectional parameters	Before	After	%Change*	P value**	r value (vs. AHI)
A					
AWAP	−30.77 ± 0.24	−30.29 ± 0.36	1.55 ± 0.94	0.130	0.101
AWAV	2.13 ± 0.006	2.14 ± 0.05	0.49 ± 0.78	0.632	0.060
B					
AWAP	−34.62 ± 0.47	−33.95 ± 0.64	1.99 ± 0.76	0.032†	0.202
ΔP	3.85 ± 0.37	3.66 ± 0.35	−5.24 ± 1.58	0.014†	0.396
AWAV	3.46 ± 0.12	3.43 ± 0.11	−0.92 ± 0.69	0.203	
C					
AWAP	−153.54 ± 6.18	−69.95 ± 2.50	53.65 ± 2.57	0.000†	0.922
ΔP	122.77 ± 6.24	39.66 ± 2.33	−66.81 ± 2.56	0.000†	0.928
AWAV	13.02 ± 0.57	7.79 ± 0.42	−42.07 ± 2.89	0.000†	0.946
D					
AWAP	−107.14 ± 4.48	−51.23 ± 1.97	51.37 ± 2.87	0.000†	0.863
ΔP	76.38 ± 4.55	20.94 ± 1.89	−71.79 ± 3.23	0.000†	0.874
AWAV	3.61 ± 0.17	3.29 ± 0.25	−9.59 ± 3.69	0.026†	0.267
E					
AWAP	−134.12 ± 4.89	−68.35 ± 3.52	48.44 ± 3.13	0.000†	0.858
ΔP	103.35 ± 4.99	38.06 ± 3.46	−62.57 ± 3.64	0.000†	0.865
AWAV	2.87 ± 0.13	2.86 ± 0.12	−0.27 ± 1.28	0.802	0.062

AWAP = area-weighted average pressure; ΔP = pressure drop; AWAV = area-weighted average velocity.
*Postoperative rate of change relative to the preoperative variable.
**Based on paired *t*-test.
† Statistically significant ($p < .05$).

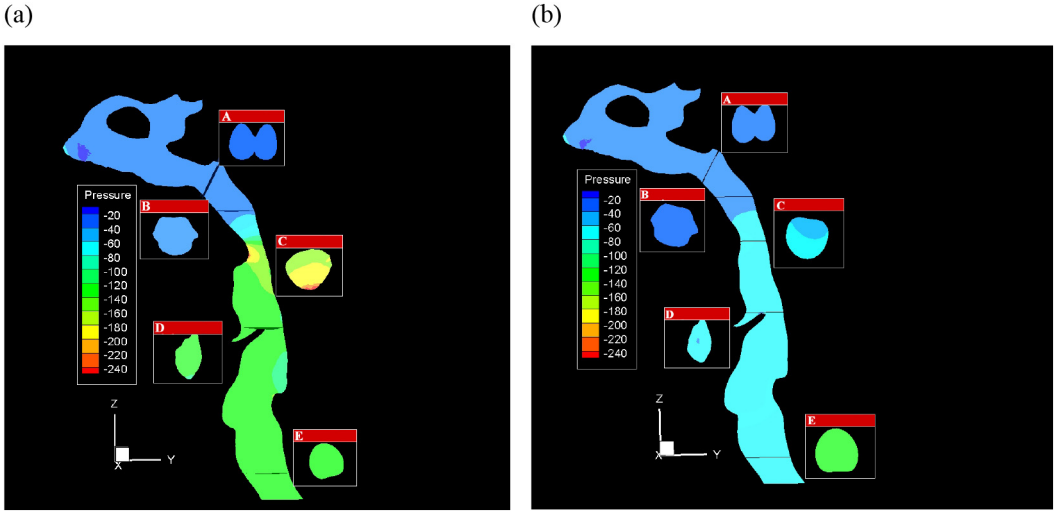

Fig. 2. Representative distribution of pressure at the median sagittal plane and cross-sections (a) before and (b) after H-UPPP. Colors used to indicate the magnitude of the pressure range from red (lowest pressure) to blue (highest pressure). (For interpretation of the references to colour in this figure legend, the reader is referred to the web version of this article.)

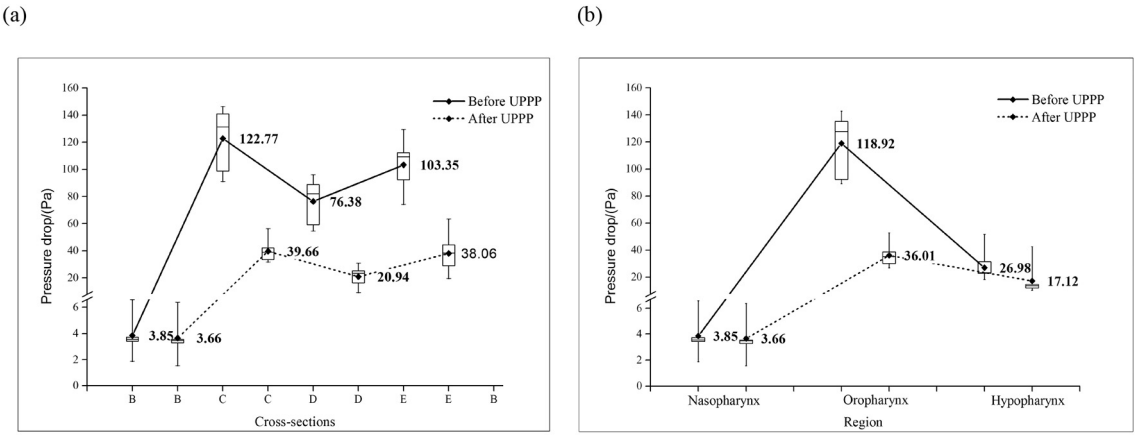

Fig. 3. (a) Comparison of pressure drop from the choana to each transverse plane before and after H-UPPP. (b) Comparison of pressure drop from each pharyngeal region before and after H-UPPP. The bottom and top sides of the box represent the 25th and 75th percentile, which is bisected by the median value; the black diamond represents the mean value and the; whiskers are used to represent the upper and lower values.

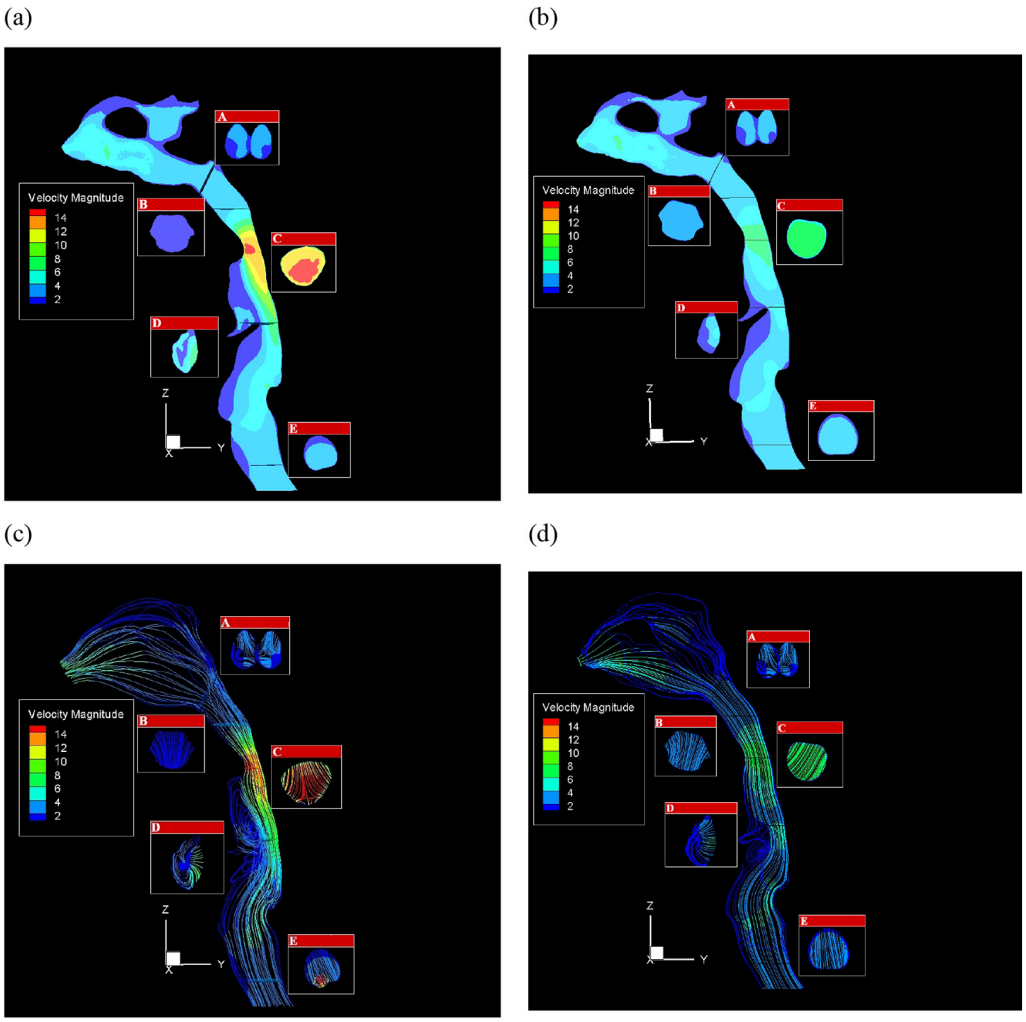

Fig. 4. A typical distribution of velocity and streamlines (colored by airflow velocity) at the median sagittal plane and cross-sections (a, c) before and (b, d) after H-UPPP. Colors are used to indicate the magnitude of velocity ranging from red (highest velocity) to blue (lowest velocity). (For interpretation of the references to colour in this figure legend, the reader is referred to the web version of this article.)

of the fitted lines of the ΔP-Q curves. The mean slopes of three pharyngeal regions demonstrated a significant increase compared the preoperative values. The oropharyngeal region demonstrated the largest shift of slope (from 88.91 to 29.26 Pa·s/L) before and after H-UPPP. In addition, a trend of decreased and discrete wall shear stress indirectly suggested the reduction of airway resistance (Fig. 6).

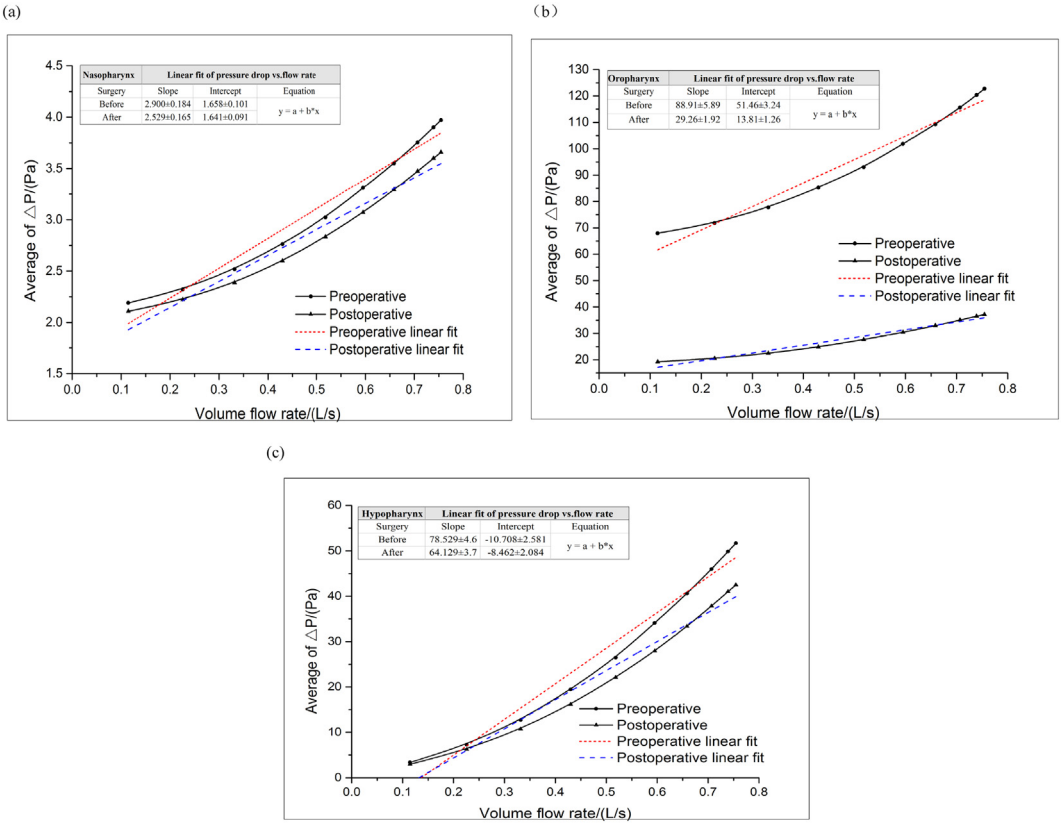

Fig. 5. The pre- and post-operative △P-Q curves and their respective the fitting lines at nasopharynx (a), oropharynx (b) and hypopharynx (c). The slope (Pa*s/L)) of the fitting line of △P-Q curves represents the effective airway resistance.

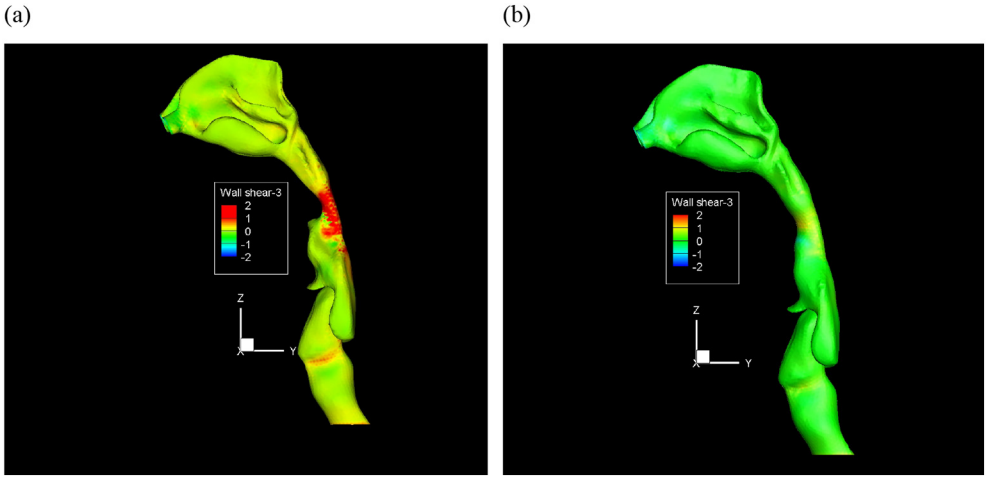

Fig. 6. A representative contour of wall shear stress from an OSAS patient (a) before and (b) after H-UPPP. Red indicates the largest friction and blue indicates the smallest friction. (For interpretation of the references to colour in this figure legend, the reader is referred to the web version of this article.)

4. Discussion

OSAS is a chronic condition characterized by the repeated collapse of the upper airway during sleep [27]. It is associated with a number of morbidities as well as diminished quality of life. UPPP is a well established surgical approach for the management of OSAS that was first introduced in 1981 [28]. Nevertheless, this technique suffered from long term side-effects including velopharyngeal insufficiency and dysphagia [9]. Therefore, H-UPPP was developed leading to better therapeutic outcomes [8–10]. The impact of UPPP on the upper airway has been previously investigated with dynamic MR imaging or 3D CT scans [11,12]. However, those imaging techniques could not investigate functional variations among other parameters like pressure, air velocity, and fluid pattern. Therefore, we used CFD model endpoints based on pressure drop to investigate airway morphology and volume after H-UPPP.

Langin et al. previously demonstrated the increased width of the upper airway after UPPP by CT measurements [29]. In our study, morphological changes also included the widening of the constricted velopharynx following H-UPPP and the cross-sectional area was closely associated with the AHI compared to the other parameters. Following H-UPPP, airway expansion led to marked improvement of the pharyngeal stenosis in the whole upper airway. However, unexpectedly, we observed that not all pharyngeal regions had significant expansions in

volume. This could be attributed to the shifting of the tongue root from anterior to posterior positions after H-UPPP. Schwab et al. previously demonstrated that UPPP led to an increase in the lateral airway dimension and a decrease in the thickness of the lateral pharyngeal walls [30]. Further, Nishimura et al. proposed that the presence of the bilateral tonsils was important for maintaining the lingual radix in a forward position [12]. Additionally, they revealed that the tongue base moved backwards after removal of tonsils following UPPP that led to the reduction of anteroposterior pharyngeal size [12]. Consequently, the rise in the lateral airway size versus the decline in the anteroposterior pharyngeal dimension could possibly be responsible for the insignificant variation of airway volume.

Analysis of our CFD model revealed a decrease of the negative pressure from all monitored planes in the postoperative models, therefore suggesting the reduction of airway collapse and occlusion during inspiration. This could be attributed to the expansion of the previously constricted airway by H-UPPP which in turn provides a better air flow environment reflected by the difference in pressure distribution (See Fig. 2). Sittitavornwong et al. previously reported that extreme airway stenosis causes significant airway resistance that could be overcome by applying more pressure (ΔP) to enable the inspiration of the normal air amount [17]. Upon the expansion of the constricted airway by surgical intervention, a decrease in airway resistance is usually observed accompanied by a decline of the required pressure during natural inspiration. Ultimately, this promotes a significant decrease in the workload of breathing resulting in an easier inspiration and improvement of the overall quality of sleep. Similarly, our results support the same notion. Our results indicate that H-UPPP improves OSAS through the decrease of ΔP, either from choana to each transverse plane or from pharyngeal regions (the sharpest decline was observed at the pre-operative site showing the minimum cross-sectional area). The decline in ΔP was significantly correlated with AHI improvement. Subsequently, the increase of airway dimension by H-UPPP led to the reduction of the airway resistance and wall shear stress. This model is a potential mechanism underlying treatment of OSAS by H-UPPP [15,17,23,26].

Fluid velocity is inversely proportional to the radius of a conduit, thus airflow velocity will decrease with the increase of the airway caliber [25]. Consistent with this idea, our findings indicate that the airflow velocity was significantly reduced at the pre-operative constricted area and at the superior border of epiglottis. However, the inspiration speed in the other three planes was not significantly changed. It is possible that H-UPPP may increase the caliber of oropharyngeal region without affecting the other regions. Alternatively, the decline in the negative pressure could lead to the observed deceleration of the airflow in accordance with Bernoulli's principle [31]. Following H-UPPP, the dilation of the narrowest area led to fluid field deceleration at the oropharynx which prevented the oropharyngeal jet from reversing upstream and circulating vertically, subsequently inhibiting the development of swirl flow [32]. Therefore, H-UPPP might have created a shift of fluid pattern from swirl to laminar flow below the most constricted region of the oropharynx [32].

In this study, we investigated the impact of H-UPPP on the upper airway using CFD. Nevertheless, the present study had few limitations that include: (1) The selection of laminar rather than turbulent airflow to mimic the airflow pattern in our flow simulation model which might affect the model accuracy. (2) CT scans were performed on fully awake patients; therefore the approximation of static airway models and absence of neural compensatory reflexes can affect the accuracy of the CFD model. (3) Patients with hypopharyngeal obstruction were not included in this study. (4) The relatively small study population. (5) Definition of the upper airway as a rigid model does not match its characteristics as a flexible model with surrounding tissues as tongue and soft palate. Future studies should focus on enhancing the accuracy of our CFD model by means of fluid-structure coupled algorithms and the recruitment of more OSAS patients.

5. Conclusion

In the present study, we demonstrated a potential therapeutic mechanism of H-UPPP based on morphology and aerodynamics. H-UPPP successfully expanded the constricted region of the velopharynx, which provides a better flow environment. Further, H-UPPP decreased the airway resistance which had a beneficial impact on the breathing workload and facilitated natural inspiration, In conclusion, results obtained from this study will be instrumental in the development of personalized virtual surgical planning which will accurately predict the efficacy of H-UPPP.

Funding

No funding was received for this research.

Conflict of interest

All authors certify that they have no affiliations with or involvement in any organization or entity with any financial interest, or non-financial interest relevant to materials discussed in this manuscript.

References

[1] Kim SJ, et al. Changes in the reflux symptom index after multilevel surgery for obstructive sleep apnea. Clin Exp Otorhinolaryngol 2017;10(3):259–64.
[2] Punjabi NM. The epidemiology of adult obstructive sleep apnea. Proc Am Thorac Soc 2008;5(2):136–43.
[3] Spicuzza L, Caruso D, Di Maria G. Obstructive sleep apnoea syndrome and its management. Ther Adv Chron Dis 2015;6(5):273–85.
[4] Chen BY, He QY. The clinical investigation and research strategy of obstructive sleep apnea-hypopnea syndrome in China. Zhonghua Jie He He Hu Xi Za Zhi 2006;29(4):217–8.
[5] Jennum P, Riha RL. Epidemiology of sleep apnoea/hypopnoea syndrome and sleep-disordered breathing. Eur Respir J 2009;33(4):907–14.
[6] de Oliveira Almeida MA, et al. Treatment of obstructive sleep apnea and hipoapnea syndrome with oral appliances. Braz J Otorhinolaryngol 2006;72(5):699–703.
[7] Caples SM, et al. Surgical modifications of the upper airway for obstructive sleep apnea in adults: a systematic review and meta-analysis. Sleep 2010;33(10):1396–407.
[8] MacKay SG, et al. Modified uvulopalatopharyngoplasty and coblation channeling of the tongue for obstructive sleep apnea: a multi-Centre Australian trial. J Clin Sleep Med 2013;9:117–24.
[9] Mantovani M, et al. Should we stop performing uvulopalatopharyngoplasty? Ind J Otolaryngol Head Neck Surg 2014;67(S1):161–2.
[10] Yang HB, Wang Y, Dong MM. Effect of Han-uvulopalatopharyngoplasty on flow-mediated dilatation in patients with moderate or severe obstructive sleep apnea syndrome. Acta Otolaryngol 2012;132(7):769–72.
[11] Bhawna, et al.. Role of dynamic MR imaging in obstructive sleep apnoea. Ind J Otolaryngol Head Neck Surg 2008;60(1):25–9.
[12] Nishimura Y, et al. Volumes of velopharyngeal and glossopharyngeal airway were not changed after Uvulopalatopharyngoplasty: report of three cases. Case Rep Otolaryngol 2016;2016:1–5.
[13] Wootton DM, et al. Computational fluid dynamics endpoints to characterize obstructive sleep apnea syndrome in children. J Appl Physiol 2013;116(1):104–12.
[14] Zheng Z, et al. Computational fluid dynamics simulation of the upper airway response to large incisor retraction in adult class I bimaxillary protrusion patients. Sci Rep 2017;7:45706.
[15] Fan Y, Cheung LK. Computational fluid dynamics analysis on the upper airways of obstructive sleep apnea using patient – specific models. IAENG Int J Comput Sci 2011;38:401–8.
[16] Fan Y, et al. Computational study on obstructive sleep apnea syndrome using patient – specific models. 2011.
[17] Sittitavornwong S, et al. Computational fluid dynamic analysis of the posterior airway space after maxillomandibular advancement for obstructive sleep apnea syndrome. J Oral Maxillofac Surg 2013;71(8):1397–405.
[18] Han D, et al. Revised uvulopalatopharyngoplasty with uvula preservation and its clinical study. ORL J Otorhinolaryngol Relat Spec 2005;67(4):213–9.
[19] Ricketts RM, Schulhof RJ, Bagha L. Orientation-sella-nasion or Frankfort horizontal. Am J Orthod 1976;69(6):648–54.
[20] Wootton DM, et al. Computational fluid dynamics upper airway effective compliance, critical closing pressure, and obstructive sleep apnea severity in obese adolescent girls. J Appl Physiol 2016;121(4):925–31.
[21] Passali D, et al. The role of rhinomanometry, acoustic rhinometry, and mucociliary transport time in the assessment of nasal patency. Ear Nose Throat J 2000;79(5):397–400.
[22] Corley RA, et al. Comparative computational modeling of airflows and vapor dosimetry in the respiratory tracts of rat, monkey, and human. Toxicol Sci

2012;128(2):500–16.
[23] Cheng GC, et al. Assessment of surgical effects on patients with obstructive sleep apnea syndrome using computational fluid dynamics simulations. Math Comput Simul 2014;106:44–59.
[24] Kim T, et al. Change in the upper airway of patients with obstructive sleep apnea syndrome using computational fluid dynamics analysis. J Craniofac Surg 2015;26(8):e765–70.
[25] Yang C, Woodson BT. Upper airway physiology and obstructive sleep-disordered breathing. Otolaryngol Clin North Am 2003;36(3):409.
[26] Liu Y, et al. Flow oscillation—a measure to predict the surgery outcome for obstructed sleep apnea (OSA) subject. J Biomech 2012;45(13):2284–8.
[27] Eckert DJ, Malhotra A. Pathophysiology of adult obstructive sleep apnea. Proc Am Thorac Soc 2008;5(2):144–53.
[28] Fujita S, et al. Surgical correction of anatomic abnormalities in obstructive sleep apnea syndrome: uvulopalatopharyngoplasty. Otolaryngol Head Neck Surg 1981;89(6):923–34.
[29] Langin T, et al. Upper airway changes in snorers and mild sleep apnea sufferers after uvulopalatopharyngoplasty (UPPP). Chest 1998;113(6):1595–603.
[30] Schwab RJ, et al. Upper airway and soft tissue anatomy in normal subjects and patients with sleep-disordered breathing. Significance of the lateral pharyngeal walls. Am J Respir Crit Care Med 1995;152(5 Pt 1):1673–89.
[31] Schwab RJ, Remmers JE, Kuna ST. Roth T, Dement WC, editors. Chapter 101 - anatomy and physiology of upper airway obstruction A2 - Kryger, Meir H, in principles and practice of sleep medicine. 5th ed.Philadelphia: W.B. Saunders; 2011. p. 1153–71.
[32] Yamamoto T, et al. Mechanisms underlying improvement in obstructive sleep apnea syndrome by Uvulopalatopharyngoplasty. Case Rep Otolaryngol 2017;2017:1–5.